IEEE Access
Multidisciplinary ⋮ Rapid Review ⋮ Open Access Journal

Received November 28, 2019, accepted December 23, 2019, date of publication January 3, 2020, date of current version January 14, 2020.

Digital Object Identifier 10.1109/ACCESS.2020.2963937

Polarimetric Calibration Scheme Combining Internal and External Calibrations, and Experiment for Gaofen-3

WEIBIN LIANG[1], ZENGZENG JIA[1], JUN HONG[2], QINGJUN ZHANG[3], AICHUN WANG[4], AND ZHAOGUO DENG[1]

[1]Key Laboratory of Technology in Geo-Spatial Information Processing and Application System, Institute of Electronics, Chinese Academy of Sciences, Beijing 100190, China
[2]National Key Laboratory of Science and Technology on Microwave Imaging, Institute of Electronics, Chinese Academy of Sciences, Beijing 100190, China
[3]Beijing Institute of Space System Engineering, China Academy of Space Technology, Beijing 100086, China
[4]China Center for Resources Satellite Data and Application, Beijing 100094, China

Corresponding author: Weibin Liang (lwbleo@126.com)

This work was supported in part by the project of the GaoFen-3 SAR calibration processing system under Grant Y5H2980402, which was funded by the China Center for Resources Satellite Data and Application.

ABSTRACT The parameters for polarization distortion of spaceborne polarimetric synthetic aperture radar (SAR) have range-dependence (or look-angle-dependence), which requires a polarimetric calibration to be performed at any look-angle. It is a huge endeavor to rely solely on ground experiments to obtain a polarimetric calibration at all look-angles. For SAR with phased array antennas we deduce, based on the model for the general polarimetric system, the model for fine polarization distortion described by the parameters of the radar device under the condition of high polarization isolation. We point out the mechanism that causes both variable and constant polarization distortions, and we deduce the correction algorithms for the two types of polarization distortion. Then we propose a polarimetric calibration scheme combining internal and external calibrations to calibrate the two types of polarization distortions for SAR with phased array antennas. The scheme uses the internal calibration data of the radar and the model of the antenna pattern established before satellite launch to invert the in-orbit antenna patterns to correct for the variable polarization distortion, and it needs only a small amount of calibration equipment to solve for the parameters for constant polarization distortion. The scheme no longer depends on the distributed target and improves the polarization precision of the data. It is applied to the calibration experiment for the data processing of the GaoFen-3 satellite and has achieved good results in applications.

INDEX TERMS Synthetic aperture radar (SAR), polarimetric calibration, polarimetric correction, polarimetric system model, internal calibration, external calibration, GaoFen-3.

I. INTRODUCTION

In the last three decades many polarimetric SAR systems have been constructed, including airborne polarimetric SAR [1]–[13] and spaceborne polarimetric SAR such as SIR-C [6], [7], [14], ALOS-1 [15]–[19]/ALOS-2 [20], [21], and RadarSat-2 [22]–[24]. To extract relevant information about the observed target and make full use of the data from the polarimetric radar, polarimetric calibration must focus on the removal of the polarimetric distortion.

Generally speaking, at present there are three main kinds of polarimetric calibration methods: 1) methods based on point targets with known scattering matrices [1], [25]; 2) methods based on distributed targets with known scattering characteristics [26], [27]; and 3) methods based on the combination of point targets and distributed targets [4], [28], [29]. In the past few decades the practice of polarimetric calibration has often adopted combined calibration methods and strategies. SIR-C/X-SAR carried out calibration tests in the Raco Calibration Field in the United States in April and October 1994. The point targets method and the method based on the distributed targets are used for polarimetric calibration; and the differential Mueller matrix of the distributed targets is measured by the polarimetric scatterometer. The results show that the parameters of the polarimetric distortion matrix vary with the look-angle of the beam [14], [30]–[32]. As one

The associate editor coordinating the review of this manuscript and approving it for publication was Michele Nappi.

of the L-band SAR systems, ALOS/PALSAR, launched by Japan in 2006, carried out many calibration experiments. These calibration experiments mainly adopted the method of combining artificial point targets with the tropical rainforest. They used the calibration field data of the Mongolia Calibration Field, the Sweden Calibration Field, DLR's Oberpfaffenhofen Calibration Field of Germany, and the Ottawa Calibration Field of Canada [15], [17], [33]. RADARSAT-2 is a C-band fully polarimetric high-resolution spaceborne SAR launched by Canada in February 2007. The polarimetric calibration scheme of RADARSAT-2 mainly combined artificial point targets and the tropical rain forest. In this method the Polarimetric Active Radar Calibrator (PARC) was used for polarimetric crosstalk calibration and for absolute calibration of the radar system, while the tropical forest data were used to estimate the imbalance of the system channel [22], [24], [34]. Gimeno *et al.* of the INTA Radar Laboratory in Spain conducted a polarimetric calibration experiment by using the TerraSAR-X full-polarimetry data in Barrax, Spain in July 2011. They combined artificial point targets and distributed targets to achieve the calibration parameters. The distributed targets in the calibration field were calibrated based on the improved Quegan method for polarimetric crosstalk, and the artificial point targets were used for imbalance calibration of channels and for absolute calibration.

Parameters for Polarimetric distortion of spaceborne SAR will vary from beam to beam, as well as with look-angle across each beam [34]–[36]; that is, the parameters for polarimetric distortion are range-dependent (or look-angle-dependent), or have range-dependence. To solve this problem the above-mentioned spaceborne SARs used a method that combined distributed targets and point targets for polarimetric calibration. This requires certain assumptions about the distributed target or requires accurate measurement of the distributed target using a scatterometer. These assumptions will result in a lower calibration accuracy, and the measurement will require additional equipment and involve a lot of work. Also, commonly used distributed targets such as tropical rain forests are subject to increasing damage, which will affect the work of calibration tests. In general these methods are based entirely on external calibration.

GaoFen-3 (GF-3) is China's first meter-level multi-polarization SAR satellite with scientific and commercial applications, which was launched in August 2016. The GF-3 has two polarization modes: QPS-I and QPS-II. The QPS-I has 28 beams; the look-angle changes from 18.9° to 42.75°; and each beam corresponds to an image width of 30 kilometers. The QPS-II has 16 beams; the look-angle changes from 18.8° to 42°; and each beam corresponds to an image width of 40 kilometers. In order to obtain high-precision polarimetry data from GF-3, we must meet the challenge to extract the parameters for polarimetric distortion from all beams and all look-angles of each beam. For GF-3, unlike the above-mentioned satellites' simple external calibration schemes, we propose a completely new solution in this paper:

1) By starting with the general polarimetric system model [2], [37], we establish a model for the polarimetric system that includes a look-angle variable, deduces the model for polarization distortion described by parameters for the radar device under the condition of high polarization isolation, and points out the mechanism for causing different types of polarization distortion. Correction algorithms for variable polarization distortion and constant polarization distortion are given. The model for polarization distortion and the correction algorithms have universal significance and can be used for research into various methods for polarimetric calibration for SAR with the phased array antennas.
2) On this basis a strategy for polarimetric calibration that combines internal and external calibrations is presented. The correction of the variable polarization distortion is obtained by inverting the in-orbit antenna patterns through the internal calibration data and the model for the antenna pattern which was established before satellite launch. An improved method for polarimetric calibration based on three PARCs obtains parameters for residual polarization distortion that correct for constant polarization distortion. The combined strategy needs only one set of polarimetric calibration equipment, which greatly reduces the need for calibration equipment and external field calibration experiments. Under the condition that the system stability meets the requirements, each beam needs to perform only one polarimetric experiment, and thus the corresponding parameters for polarization distortion can be obtained.
3) The data processing results of the GF-3 satellite polarimetric calibration experiments show that the strategy can do a good job of correcting the two types of polarization distortion and greatly improve the polarization precision of the data; and it no longer relies on distributed targets such as tropical rain forests.

In part II of this paper a model for a polarimetric system with look-angle variable is constructed, and two types of correction algorithms for polarization distortion are deduced. Section III gives the polarimetric calibration scheme for the combination of internal and external calibration. In Section IV the GF-3 SAR satellite and the external field calibration experiments are described, then the experimental data from the polarimetric calibration are processed and analyzed. Part V is the conclusion.

II. THE VARIABLE AND CONSTANT POLARIZATION DISTORTIONS AND THE CORRECTION METHODS

A. CLASSIFICATION OF POLARIZATION DISTORTIONS

1) THE POLARIMETRIC DISTORTION VARIATION MECHANISM WITH ANGLES

At present the architecture of most airborne and spaceborne polarimetric radars [38] is shown in Figure 1 [37], [38]. The polarimetric radar alternately transmits H-polarized and

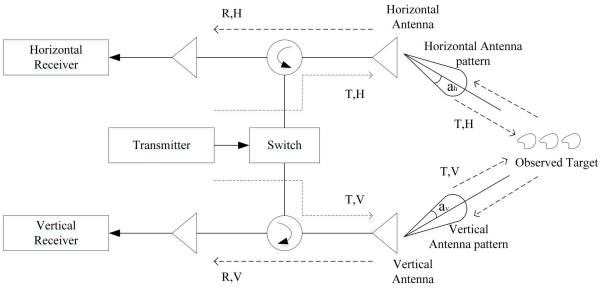

FIGURE 1. **The operating principle of polarization system.**

V-polarized signals while working, and then the H-polarized antenna and V-polarized antenna simultaneously receive echo signals. After sampling by the two receivers four kinds of polarimetric echo data are formed, including HH, HV, VH and VV.

According to the strip SAR echo acquisition process and imaging mechanism, we know that the amplitude and phase characteristics of the SAR imaging processor vary with the look-angle, and the main reasons for this result include:

1) The echo signals of the targets at different look-angles have different weights according to the antenna pattern.
2) The targets at different look-angles have different echo power attenuation due to different slant ranges.
3) Due to the unevenness of the atmosphere and its changes with time, the attenuation of the image at different azimuth angles and look-angles is different.

The above three factors will cause the response characteristics of the single-channel SAR system to spatially vary, resulting in different responses of the targets with the same scattering characteristics at different imaging positions. The polarization distortion of fully polarimetric SAR is related to the spatial variation of the response characteristics of a single channel SAR, but it is not the same, as follows:

1) The consistent change of the antenna patterns with the look-angle for different polarimetric channels does not cause the polarization distortion to change with the look-angle. Only inconsistent changes in the antenna pattern of each channel will cause the polarization distortion to change with the look-angle. Since the H- and the V-polarized antennas are independent, it is almost impossible for the amplitude-phase characteristics of the patterns for different channels to change consistently with the look-angle, which inevitably causes polarization distortion to vary with the look-angles.
2) The power attenuation introduced by the slant range has the same effect on different polarization channels and does not cause the range-dependence of polarization distortion.
3) Because of the in-homogeneous distribution of the atmosphere, the variation with time, the effects of the ionospheric and other complex components, the effects on different polarization channels are different and change with position, which will lead to a certain degree of spatial variation of polarization distortion.

Among these factors the effect of atmosphere is relatively small, and it is also difficult to accurately measure the state of the atmosphere at all positions in real time. Usually the spatial variation caused by the atmosphere is neglected and considered to be a random error. Under this condition, for strip mode SAR, the spatial variation of polarization distortion is mainly due to range direction. Therefore, the antenna patterns are the main factor in the range-dependence of polarization distortion.

2) THE POLARIMETRIC SYSTEM MODEL CONSIDERING THE RANGE-DEPENDENCE

For the specific look-angle of a specific beam the classical model for a polarimetric system of polarimetric SAR under linear conditions [1], [2], [37], [38] is given by Equation (1):

$$\begin{aligned} M &= Ae^{j\varphi}R^tST + N \\ &= Ae^{j\varphi}\begin{pmatrix} 1 & \delta_2 \\ \delta_1 & f_1 \end{pmatrix}\begin{pmatrix} S_{11} & S_{12} \\ S_{21} & S_{22} \end{pmatrix}\begin{pmatrix} 1 & \delta_3 \\ \delta_4 & f_2 \end{pmatrix} \\ &\quad + \begin{pmatrix} N_{11} & N_{12} \\ N_{21} & N_{22} \end{pmatrix} \end{aligned} \tag{1}$$

In the formula a measured scattering matrix $M = \begin{pmatrix} M_{11} & M_{12} \\ M_{21} & M_{22} \end{pmatrix}$ is related to an actual target scattering matrix $S = \begin{pmatrix} S_{11} & S_{12} \\ S_{21} & S_{22} \end{pmatrix}$; A represents the radar system's gains and losses (in amplitude), and φ is any phase shift due to the round-trip delay between the target and radar and any losses in the system. The normalized receiving and transmitting matrices $R = \begin{pmatrix} 1 & \delta_1 \\ \delta_2 & f_1 \end{pmatrix}$ and $T = \begin{pmatrix} 1 & \delta_3 \\ \delta_4 & f_2 \end{pmatrix}$ describe the relative polarimetric characteristics of the radar system and signal transmission processes, including among others the radar transmitter, transmit antenna, receive antenna, receiver, gain controller, and ionosphere. The matrix $N = \begin{pmatrix} N_{11} & N_{12} \\ N_{21} & N_{22} \end{pmatrix}$ represents the additive noise voltage present in each radar channel. The subscripts 1 and 2 correspond to H and V polarizations. f_1 and f_2 are channel imbalance terms for receivers and transmitters, respectively, and δ_i $(i = 1, 2, 3, 4)$ is the cross-talk term representing the cross-polarization isolation of the system.

For practical polarimetric radars, such as the GF-3 satellites, due to the non-linearity introduced by their working mechanisms and devices [37], a more general model for the polarimetric system is needed, which was first proposed by Freeman in 1991 in [2]. While in the process of studying GF-3 satellite calibration, Liang improved Freeman's general model of the polarimetric system into 2×2 matrix form through simple mathematical transformation [37] given by Equation (2):

$$\bar{M} = \begin{pmatrix} M_{11} & M_{12} \\ \gamma \cdot M_{21} & M_{22} \end{pmatrix} = Ae^{j\varphi}R^tST + N \tag{2}$$

where the γ factor is a parameter introduced by Freeman for correcting the non linearity of the radar polarimeter. It is

a measure of the product of the gain error terms in the co-pol channels versus the cross-pol [2] channels and is the ratio of the system transfer functions' product of the co-pol channels versus the the system transfer functions' product of the cross-pol, and is the new imbalance factor [37] given by Equation (3):

$$\gamma = \frac{H_{11}^s H_{22}^s}{H_{21}^s H_{12}^s} \tag{3}$$

where H_{pq}^s represents the system transfer function of the pq channel. The corrected measured matrix $\bar{M}$ is called a co-pol versus cross-pol balanced measured matrix of the radar polarimeter [37].

The γ factor is a parameter introduced by the non linearity of the radar polarimeter (for example, the Manual Gain Control (MGC) which sets value switching introduces errors when operating in different channels) and is independent of the look-angles, and therefore has no range-dependence (further explanation will be given later). The other six polarimetric parameters, f_1, f_2 and δ_i $(i = 1, 2, 3, 4)$, vary with the look-angle and have a range-dependence.

Introducing the look-angle variable and ignoring the additive noise, the more general expression of the above model for the general polarimetric system is given by Equation (4):

$$\begin{aligned}\bar{M} &= \begin{pmatrix} M_{11}(\alpha) & M_{21}(\alpha) \\ \gamma \cdot M_{12}(\alpha) & M_{22}(\alpha) \end{pmatrix} = Ae^{j\varphi} R^t S T \\ &= A(\alpha)e^{j\varphi(\alpha)} \begin{pmatrix} 1 & \delta_2(\alpha) \\ \delta_1(\alpha) & f_1(\alpha) \end{pmatrix} \\ &\quad \cdot \begin{pmatrix} S_{11} & S_{12} \\ S_{21} & S_{22} \end{pmatrix} \begin{pmatrix} 1 & \delta_3(\alpha) \\ \delta_4(\alpha) & f_2(\alpha) \end{pmatrix} \\ &= A(\alpha)e^{j\varphi(\alpha)} \begin{pmatrix} 1 & 0 \\ 0 & f_1(\alpha) \end{pmatrix} S' \begin{pmatrix} 1 & 0 \\ 0 & f_2(\alpha) \end{pmatrix}\end{aligned} \tag{4}$$

where α is the look-angle of the range antenna patterns corresponding to the observed target and is an independent variable. The relationship between S and S' is given by Equation (5):

$$\begin{aligned}S' &= \begin{pmatrix} S'_{11}(\alpha) & S'_{12}(\alpha) \\ S'_{21}(\alpha) & S'_{22}(\alpha) \end{pmatrix} \\ &= \begin{pmatrix} 1 & \delta_2(\alpha) \\ \delta_1(\alpha)/f_1(\alpha) & 1 \end{pmatrix} \begin{pmatrix} S_{11} & S_{12} \\ S_{21} & S_{22} \end{pmatrix} \\ &\quad \cdot \begin{pmatrix} 1 & \delta_3(\alpha)/f_2(\alpha) \\ \delta_4(\alpha) & 1 \end{pmatrix}\end{aligned} \tag{5}$$

At present for general radar polarimeters with phased array antennas the polarization isolation can reach more than 30 dB, so the cross-talk factors δ_1, δ_2, δ_3 and δ_4 are small. The variation of each cross-talk factor with look-angles is smaller relative to the cross-talk factor itself. The characteristic that each imbalance factor varies with the look-angles is that the amplitude fluctuates around one over a small range, and the phase deviates from zero to a significant value, but the range of fluctuation is also small. So the variation of the imbalance factors has little effect on the cross-talk factors $\delta_1(\alpha)/f_1(\alpha)$ and $\delta_3(\alpha)/f_2(\alpha)$ in terms of amplitude characteristics. So the spatial variation of the cross-talk factors can be ignored, and the cross-talk factors δ_2, δ_4, $\delta_1(\alpha)/f_1(\alpha)$, and $\delta_3(\alpha)/f_2(\alpha)$ can be seen as constant according to Equation (6):

$$\begin{aligned}S' &\doteq \begin{pmatrix} 1 & \delta_2 \\ \delta_1/f_1 & 1 \end{pmatrix} \begin{pmatrix} S_{11} & S_{12} \\ S_{21} & S_{22} \end{pmatrix} \begin{pmatrix} 1 & \delta_3/f_2 \\ \delta_4 & 1 \end{pmatrix} \\ &= \begin{pmatrix} S'_{11} & S'_{12} \\ S'_{21} & S'_{22} \end{pmatrix}\end{aligned} \tag{6}$$

S' is substituted into the model for the general polarimetric system as given by Eq. (4) and expanded. Results are obtained as Equations (7) to (10):

$$M_{11}(\alpha) \doteq A(\alpha)e^{j\varphi(\alpha)} S'_{11} = H_{11}^s(\alpha) S'_{11}, \tag{7}$$

$$M_{12}(\alpha) \doteq f_2(\alpha)A(\alpha)e^{j\varphi(\alpha)} S'_{12} = H_{12}^s(\alpha) S'_{12}, \tag{8}$$

$$M_{21}(\alpha) \doteq (f_1(\alpha)/\gamma)A(\alpha)e^{j\varphi(\alpha)} S'_{21} = H_{21}^s(\alpha) S'_{21}, \tag{9}$$

$$M_{22}(\alpha) \doteq f_1(\alpha)f_2(\alpha)A(\alpha)e^{j\varphi(\alpha)} S'_{22} = H_{22}^s(\alpha) S'_{22}, \tag{10}$$

where $H_{11}^s(\alpha) = A(\alpha)e^{j\varphi(\alpha)}$, $H_{12}^s(\alpha) = f_2(\alpha)A(\alpha)e^{j\varphi(\alpha)}$, $H_{21}^s(\alpha) = (f_1(\alpha)/\gamma)A(\alpha)e^{j\varphi(\alpha)}$ and $H_{22}^s(\alpha) = f_1(\alpha)f_2(\alpha)A(\alpha)e^{j\varphi(\alpha)}$ can be called the system transfer functions of the four polarimetric channels.

The above equations reflect that under the condition of high polarization isolation, the parameters with range-dependence for polarimetric distortion are mainly the receiving and transmitting channel imbalance factors f_1 and f_2. The amplitude-phase factor $A(\alpha)e^{j\varphi(\alpha)}$ has the same effect on the four polarimetric channels and does not cause polarization distortion to change with look-angle. $H_{11}^s(\alpha)$, $H_{12}^s(\alpha)$, $H_{21}^s(\alpha)$ and $H_{22}^s(\alpha)$ are substituted into Eq. (3) for the γ factor, which indicates that the γ factor does not have range-dependence; that is, $\gamma(\alpha) = \gamma$.

3) CLASSIFICATION OF POLARIZATION DISTORTIONS

According to the radar equation and radiation calibration theory [39], Equations (11) to (14) hold:

$$\begin{aligned}M_{11}(\alpha) &\doteq H_{11}^s(\alpha) S'_{11} \\ &= \frac{E_T G_{R11} G_{P11} G_{HT} G_{HR} \bar{A}_{HT}(\alpha) \bar{A}_{HR}(\alpha) \lambda}{(4\pi)^{3/2} R^2(\alpha) L_{11}} \cdot S'_{11} \\ &= K_{11} \frac{\bar{A}_{HT}(\alpha) \bar{A}_{HR}(\alpha)}{R^2(\alpha)/R_0^2} \cdot S'_{11}\end{aligned} \tag{11}$$

$$\begin{aligned}M_{12}(\alpha) &\doteq H_{12}^s(\alpha) S'_{12} \\ &= \frac{E_T G_{R12} G_{P12} G_{HT} G_{VR} \bar{A}_{HT}(\alpha) \bar{A}_{VR}(\alpha) \lambda}{(4\pi)^{3/2} R^2(\alpha) L_{12}} \cdot S'_{12} \\ &= K_{12} \frac{\bar{A}_{HT}(\alpha) \bar{A}_{VR}(\alpha)}{R^2(\alpha)/R_0^2} \cdot S'_{12}\end{aligned} \tag{12}$$

$$\begin{aligned}M_{21}(\alpha) &\doteq H_{21}^s(\alpha) S'_{21} \\ &= \frac{E_T G_{R21} G_{P21} G_{VT} G_{HR} \bar{A}_{VT}(\alpha) \bar{A}_{HR}(\alpha) \lambda}{(4\pi)^{3/2} R^2(\alpha) L_{21}} \cdot S'_{21} \\ &= K_{21} \frac{\bar{A}_{VT}(\alpha) \bar{A}_{HR}(\alpha)}{R^2(\alpha)/R_0^2} \cdot S'_{21}\end{aligned} \tag{13}$$

$$M_{22}(\alpha) \doteq H_{22}^s(\alpha) S'_{22}$$

$$= \frac{E_T G_{R22} G_{P22} G_{VT} G_{VR} \bar{A}_{VT}(\alpha) \bar{A}_{VR}(\alpha) \lambda}{(4\pi)^{3/2} R^2(\alpha) L_{22}} \cdot S'_{22}$$
$$= K_{22} \frac{\bar{A}_{VT}(\alpha) \bar{A}_{VR}(\alpha)}{R^2(\alpha)/R_0^2} \cdot S'_{22} \quad (14)$$

where E_T is the electric current intensity of the transmitting signal; G_{Rij} is the amplitude-phase gain of the ij-channel receiver; G_{Pij} is the amplitude-phase gain of the ij-channel processor; L_{ij} is the amplitude-phase gain corresponding to the system loss of the ij-channel; $A_{HT}(\alpha) = G_{HT}\bar{A}_{HT}(\alpha)$ is true value of the transmitting amplitude-phase pattern of $H-$channel antenna along the range direction, $\bar{A}_{HT}(\alpha)$ is the corresponding in-orbit measurement amplitude-phase antenna, G_{HT} is the corresponding fixed amplitude-phase deviation, including antenna gain and phase deviation, and it is a complex number; $A_{VT}(\alpha) = G_{VT}\bar{A}_{VT}(\alpha)$ is the true value of the transmitting amplitude-phase pattern of $V-$channel antenna along the range direction, $\bar{A}_{VT}(\alpha)$ is the corresponding in-orbit measurement by the amplitude-phase antenna, G_{VT} is the corresponding fixed amplitude-phase deviation; $A_{HR}(\alpha) = G_{HR}\bar{A}_{HR}(\alpha)$ is the true value of the receiving amplitude-phase pattern of $H-$channel antenna along the range direction, $\bar{A}_{HT}(\alpha)$ is the corresponding in-orbit measurement of the amplitude-phase antenna, G_{HR} is the corresponding fixed amplitude phase deviation; $A_{VR}(\alpha) = G_{VR}\bar{A}_{VR}(\alpha)$ is the true value of the amplitude-phase pattern of the $V-$channel antenna along the range direction, $\bar{A}_{VR}(\alpha)$ is the corresponding in-orbit measurement by the amplitude-phase antenna, G_{VR} is the corresponding fixed amplitude-phase deviation; R_0 is the reference range value used for slant range correction and is constant. K_{11}, K_{12}, K_{21} and K_{22} are complex constants, and they can be denoted by Equations (15) to (18):

$$K_{11} = \frac{E_T G_{R11} G_{P11} G_{HT} G_{HR} \lambda R_0^2}{(4\pi)^{3/2} L_{11}} \quad (15)$$

$$K_{12} = \frac{E_T G_{R12} G_{P12} G_{HT} G_{VR} \lambda R_0^2}{(4\pi)^{3/2} L_{12}} \quad (16)$$

$$K_{21} = \frac{E_T G_{R21} G_{P21} G_{VT} G_{HR} \lambda R_0^2}{(4\pi)^{3/2} L_{21}} \quad (17)$$

$$K_{22} = \frac{E_T G_{R22} G_{P22} G_{VT} G_{VR} \lambda R_0^2}{(4\pi)^{3/2} L_{22}} \quad (18)$$

In Eqs. (11) - (14), $\frac{\bar{A}_{HT}(\alpha)\bar{A}_{HR}(\alpha)}{R^2(\alpha)/R_0^2}$, $\frac{\bar{A}_{HT}(\alpha)\bar{A}_{VR}(\alpha)}{R^2(\alpha)/R_0^2}$, $\frac{\bar{A}_{VT}(\alpha)\bar{A}_{HR}(\alpha)}{R^2(\alpha)/R_0^2}$ and $\frac{\bar{A}_{VT}(\alpha)\bar{A}_{VR}(\alpha)}{R^2(\alpha)/R_0^2}$ are the variables that vary with the look-angle. They are the main factors for the amplitude and phase characteristics variation with look-angles. The inconsistent changes of the four variables with the look-angle are the main factors for the range-dependence of the polarization distortion. This part of the polarization distortion is a variable polarization distortion, which is called the first type of polarization distortion. The slant range $R(\alpha)$ is the same for all four channels, and the change is consistent, which will not cause the range-dependence of the polarization distortion; however, the antenna pattern items are inconsistent, which is the key factor for the range-dependence of the polarization distortion.

The inconsistency of the remaining constant terms K_{11}, K_{12}, K_{21} and K_{22} will result in uniform polarization distortion of the image of the entire scene. This part of the polarization distortion does not change with the look angle, and is a constant polarization distortion, which is the second type of polarization distortion.

B. CORRECTION METHODS OF POLARIZATION DISTORTIONS

1) CORRECTION ALGORITHM OF THE VARIABLE POLARIZATION DISTORTION

In order to eliminate the change of the response in each polarization channel with respect to the look-angle, according to Eqs. (11)-(14) we construct four functions $\frac{R^2(\alpha)/R_0^2}{\bar{A}_{HT}(\alpha)\bar{A}_{HR}(\alpha)}$, $\frac{R^2(\alpha)/R_0^2}{\bar{A}_{HT}(\alpha)\bar{A}_{VR}(\alpha)}$, $\frac{R^2(\alpha)/R_0^2}{\bar{A}_{VT}(\alpha)\bar{A}_{HR}(\alpha)}$, and $\frac{R^2(\alpha)/R_0^2}{\bar{A}_{VT}(\alpha)\bar{A}_{VR}(\alpha)}$, also called correction factors. Use these factors to multiply the image data at the corresponding look-angle of each channel, then generate a new scattering matrix M' whose expression for the four elements is updated using Equations (19) to (22):

$$M'_{11} = M_{11}(\alpha)\frac{R^2(\alpha)/R_0^2}{\bar{A}_{HT}(\alpha)\bar{A}_{HR}(\alpha)} = K_{11}S'_{11} \quad (19)$$

$$M'_{12} = M_{12}(\alpha)\frac{R^2(\alpha)/R_0^2}{\bar{A}_{HT}(\alpha)\bar{A}_{VR}(\alpha)} = K_{12}S'_{12} \quad (20)$$

$$M'_{21} = M_{21}(\alpha)\frac{R^2(\alpha)/R_0^2}{\bar{A}_{VT}(\alpha)\bar{A}_{HR}(\alpha)} = K_{21}S'_{21} \quad (21)$$

$$M'_{22} = M_{22}(\alpha)\frac{R^2(\alpha)/R_0^2}{\bar{A}_{VT}(\alpha)\bar{A}_{VR}(\alpha)} = K_{22}S'_{22} \quad (22)$$

This eliminates the variables with the look-angle and completes the correction of the variable polarization distortion; i.e., the correction of the first type of polarization distortion.

2) CORRECTION ALGORITHM OF THE CONSTANT POLARIZATION DISTORTION

After correcting the variable polarization distortion the corrected results are re-formed as a matrix. Following the model of the general polarimetric system [2], [37], we obtain Equation (23):

$$\bar{M}' = \begin{pmatrix} K_{11}S'_{11} & K_{12}S'_{12} \\ \gamma \cdot K_{21}S'_{21} & K_{22}S'_{22} \end{pmatrix} = Ae^{j\varphi}R^t ST + N \quad (23)$$

This equation is independent of the look-angle, and each item is a constant. The parameters for the polarimetric distortion, R, T, γ, and complex constant $Ae^{j\varphi}$, can be obtained by the usual polarimetric calibration method, and the residual polarization distortion can be corrected using Equation (24):

$$\hat{S} = \frac{1}{Ae^{j\varphi}}(R^t)^{-1}\bar{M}'(T)^{-1} \quad (24)$$

In this way we obtain the estimated value $\hat{S}$ of the target scattering matrix S at any look-angle, and the correction of all polarization distortion is completed.

III. COMBINATORIAL POLARIMETRIC CALIBRATION SCHEME

According to the previous derivation, the key to correcting polarization distortion depends on two aspects:

(1) Obtain the transmitting and receiving amplitude-phase antenna patterns of the H- and V-polarized channels to eliminate the range-dependence of polarization distortion;

(2) Then, solve the uniform polarization distortion parameters of the image of the whole scene for a specific beam.

A. COMBINATORIAL POLARIMETRIC CALIBRATION SCHEME

Calibration of polarized radar is a key issue that requires system consideration and design. For the spaceborne SAR of phased array antennas, the full polarization mode is generally implemented in strip mode. Under the current technical conditions polarization isolation of more than 30 dB can be achieved. For a specific beam the effect of polarization cross-talk variation is very small; that is, in the scope of a specific beam, it can be assumed that the polarization cross-talk does not change with the look-angle. Then based on the above theory, the following polarization calibration scheme can be developed:

(1) Before launch carry out a large number of test work; construct the emission pattern and the receiving pattern models of the H-polarized and V-polarized antennas, so as to obtain the accurate antenna patterns through the internal calibration monitoring data after launch.

(2) After the satellite is in orbit the polarimetric calibration equipment is arranged at the test site, and the external field calibration test is carried out for each beam, and then the polarization distortion parameters of each beam are obtained by processing the test data.

For spaceborne SAR with phased array antennas according to the current development status of in-orbit measurement technology of the antenna pattern [40]–[42], inverting the antenna pattern of each polarimetric channel is a mature technology. It uses the internal calibration data and the model of the antenna pattern established before launch, which is appropriately applied in many on-board SARs. Comprehensive and accurate measurement of the antenna pattern of each beam of the spaceborne SAR greatly reduces the time of the in-orbit test and improves the effective life of the satellite in orbit.

This polarimetric calibration scheme combines the advantages of internal and external calibrations, reducing the dependence on common distributed targets such as tropical rain forests. Each beam needs to be calibrated once over a period of time. For the field test theoretically only one set of polarimetric calibration equipment is needed, which greatly reduces the number required for the polarization calibration equipment and the workload of the external field calibration test.

B. INVERT ANTENNA PATTERN VIA INTERNAL CALIBRATION MONITORING DATA AND THE MODEL OF THE KNOWN ANTENNA PATTERN

For phased array antennas commonly used in spaceborne SAR the accurate model for the antenna is established by ground tests before launch, and the in-orbit calibration function is used to test the TR Modules (TRM) one by one. After the inversion a two-dimensional antenna pattern can be obtained. The antenna subarray is tested row by row, and inversion provides a one-dimensional range-directional antenna pattern.

By considering the exact geometrical dimensions of the antenna the model of the antenna is used to calculate radiation patterns via superposition of the measured and weighted embedded subarray patterns and beam excitation coefficients. An error matrix, which includes drifting or failed antenna elements, is determined by internal calibration loops and orthogonal code sequences applied to the TRMs [40]. The embedded subarray patterns describe the radiation characteristics of each sub-array element embedded into the whole antenna. Grafmuller *et al.* [41] presented the calculation method of the radiated pattern in elevation and azimuth as given by Equation (25):

$$\bar{A}(\alpha,\varepsilon)=\sum_{m=0}^{M-1}\sum_{n=0}^{N-1}[\bar{C}_{SA,mn}(\alpha,\varepsilon)\cdot a_{mn}\cdot E_{SA,mn}\cdot e^{jk\sin\alpha\cos\varepsilon(-\frac{N-1}{2}+n)\Delta y}\cdot e^{jk\cos\alpha\sin\varepsilon(-\frac{M-1}{2}+m)\Delta x}] \tag{25}$$

where α is the desired elevation angle, which is the look-angle; ε is the desired azimuth angle, N is the number of rows in the subarray; M is the number of columns in the subarray; the embedded subarray patterns C_{SA} are given for each row, column, elevation, and azimuth angle; a is the commanded excitation coefficient; E_{SA} is the error matrix; Δx and Δy are the inter-subarray distances, and k is inter-subarray distance [42].

By using the single-row internal calibration data to invert the one-dimensional range pattern, we obtain Equation (26):

$$\bar{A}(\alpha)=\sum_{m=0}^{M-1}[\bar{C}_{SA,m}(\alpha)\cdot a_m\cdot E_{SA,m}\cdot e^{jk\cos\alpha(-\frac{M-1}{2}+m)\Delta x}] \tag{26}$$

By measuring the single-line receive/transmit signals of the H and V polarized antenna arrays one by one, the normalized antenna pattern in elevation $\bar{A}_{HT}(\alpha)$, $\bar{A}_{VT}(\alpha)$, $\bar{A}_{HR}(\alpha)$, and $\bar{A}_{HR}(\alpha)$ can be obtained.

C. MEASURE PARAMETERS FOR UNIFORM POLARIMETRIC DISTORTION USING EXTERNAL POLARIMETRIC CALIBRATION

There are many polarimetric calibration methods based on point targets. Calibration of the polarimetric SAR that depends on the model for the general polarimetric system is based on the PARCs-based methods proposed by Freeman. The specific algorithm refers to the Freeman and Liang articles [2], [37], and the distortion parameters γ, R, and T can be obtained.

In order to improve the signal-to-noise ratio of the point targets in the polarimetric calibration experiment, the calibration equipment should be placed in the middle of the swath.

IV. POLARIMETRIC CALIBRATION EXPERIMENTS OF GF-3 AND DATA PROCESSING

A. INTRODUCTION TO GF-3

In order to meet the quantitative application of GF-3 and improve the calibration level of data, the internal calibration subsystem in GF-3 takes full account of various calibration requirements, covers the entire receiving and transmitting link, and has a variety of calibration capabilities, including fully-polarized calibration, extraction of the real linear frequency modulation signal, system gain calibration, antenna pattern, and gain monitoring. The GF-3 internal calibration subsystem has three calibration functions: continuous calibration, head and tail calibration, and imaging interpolation calibration [43]. It can meet the needs of ground test by continuous monitoring of system changes in imaging and calibration of antenna and channel parameters. Among them, head and tail calibration is the main method for subsequent use. In order to meet different calibration requirements GF-3 has designed several calibration loops, including among others noise calibration, delay reference calibration, non-delay reference calibration, and full array transceiver calibration [44].

The design of the internal calibration subsystem of GF-3 satellite and the ground test before satellite launch make it possible to acquire the data of the antenna pattern of different channels on orbit in polarization mode, and to correct the range-dependence of the parameters for the polarimetric distortion by using the internal calibration data.

B. THE EXTERNAL CALIBRATION FIELD EXPERIMENT OF GF-3

The GF-3 satellite has successfully carried out four polarimetric calibration experiments on Erdos on 8 September 2016, 19 September 2016, 11 July 2017, and 16 July 2017 [37]. These experiments involved five PARCs, nine triangular corner reflectors (TCRs), three 45° dihedral corner reflectors (DCRs), and one 0° DCR [37]. Because of the conditions surrounding the site, equipment condition, preparation time, and manpower, not all the devices participated in each test. The first experiment used five PARCs, three TCRs and three 45° DCRs; The second experiment used three PARCs, two TCRs, one 45° DCR and one 0° DCR; The third experiment used three PARCs and seven TCRs; The forth experiment used three PARCs and nine TCRs.

Due to the limitation of site conditions, all calibration equipment is distributed within a range of less than 5 kilometers in the range direction, while the whole imaging bandwidth is about 30 kilometers, which can cover part of the imaging bandwidth. Later data analysis shows that a small area can also reflect the range-dependence of polarization distortion.

C. EXPERIMENTAL RESULTS AND ANALYSIS

Before launch the ground test result shows that the polarization isolation of GF-3 global antenna is better than 35 dB [45], [46]. Evaluation of the quantity after launch also shows that the polarization isolation of GF-3 satellite can reach 35 dB, which indicates that is proposed in this paper, which is based on the neglect of the range-dependence of the cross-talk factors, can be applicable to GF-3. So the polarimetric calibration of the GF-3 satellite can adopt the above-mentioned combinatorial calibration scheme. The amplitude-phase error of the antenna patterns are obtained by using the internal calibration data and the antenna model [47]. And the parameters of the constant polarization distortion are solved by external calibration experiments with three PARCs, which is specifically given by Liang *et al.* [37].

In order to enhance the contrast and persuasiveness of the experiment, we used three polarization calibration schemes to process the experimental data. The first scheme did not use the internal calibration data to correct the measured matrix obtained by the calibration equipment; the second scheme used the internal calibration data to correct the measured matrix obtained by the calibration equipment; the third scheme uses the correction method combined with the internal calibration and external calibration proposed in this paper. In order to ensure the accuracy of the extracted scattering matrix, after finding the position of the point target on the single-look complex image of the four polarization channels, we select the area of 32 pixels $\times$ 32 pixels around the point target, and the range and the azimuth directions are respectively interpolated 128 times, and then the point target peak position is found. Extract the complex number at the position to obtain the scattering matrix of the target.

Of the four experiments described in Section IV-B, three TCRs and three 45° DCRs were used on 8 September 2016, and there were no such balanced experiment equipment configurations in the three experiments conducted on the other three dates. So as an example, we used the data of the experiment on 8 September 2016 to analyze the effects of the proposed combination scheme. The processing results of three schemes of this experiment are shown in Table 1, and M_{hh}, M_{hh}, M_{hh} and M_{hh} represent measurements of the polarization response of the four channels (HH, HV, VH and VV).

Since the ideal polarization scattering matrix of the triangular reflector is $\begin{pmatrix} 1 & 0 \\ 0 & 1 \end{pmatrix}$ [48], we normalize the measured scattering matrix by using the HH channel (element

TABLE 1. The calibration experiment data processing results on September 8, 2016.

Device ID	Channels	Normalized Matrices (no any correction)	Normalized Matrices (only internal calibration)	Normalized Matrices (combined correction)
$ARC1$	M_{hh}	0.0081∠174.9997°	0.0072∠102.9005°	0.0008∠30.4265°
	M_{hv}	0.0005∠17.262°	0.0005∠115.6957°	0.0004∠109.2795°
	M_{vh}	1∠0°	1∠0°	1∠0°
	M_{vv}	0.0197∠126.6781°	0.0192∠-51.2045°	0.0006∠46.2279°
$ARC2$	M_{hh}	0.0048∠-28.6262°	0.0043∠149.2207°	0.001∠-11.8787°
	M_{hv}	1.0∠0.0°	1.0∠0.0°	1.0∠0.0°
	M_{vh}	0.0004∠142.0635°	0.0003∠24.5702°	0.0003∠35.8663°
	M_{vv}	0.0025∠-133.1948°	0.0035∠-38.3071°	0.0009∠142.3814°
$ARC3$	M_{hh}	1.0∠0.0°	1.0∠0.0°	1.0∠0.0°
	M_{hv}	0.9126∠-166.2929°	0.9234∠18.4576°	1.0002∠-0.0119°
	M_{vh}	0.7803∠106.8238°	0.8714∠-174.0043°	1.0001∠-179.9994°
	M_{vv}	0.9278∠-66.2013°	1.0332∠-161.5746°	1∠-179.9979°
$ARC4$	M_{hh}	1.0∠0.0°	1.0∠0.0°	1.0∠0.0°
	M_{hv}	0.0049∠-93.6971°	0.0068∠93.9518°	0.0161∠106.446°
	M_{vh}	0.0066∠2.8059°	0.0068∠86.3284°	0.0082∠72.2699°
	M_{vv}	1.0018∠96.771°	1.0644∠14.7223°	1.0367∠-4.1433°
$ARC5$	M_{hh}	1.0∠0.0°	1.0∠0.0°	1.0∠0.0°
	M_{hv}	0.0042∠94.517°	0.0045∠-81.1735°	0.0064∠127.5089°
	M_{vh}	0.0073∠-101.5628°	0.0065∠-22.6291°	0.0081∠-6.618°
	M_{vv}	1.1512∠136.379°	1.035∠29.8275°	1.0083∠10.9789°
$TCR1$	M_{hh}	1.0∠0.0°	1.0∠0.0°	1.0∠0.0°
	M_{hv}	0.0181∠59.6706°	0.0181∠-110.0032°	0.019∠-160.1919°
	M_{vh}	0.0144∠176.3157°	0.016∠-107.5421°	0.0166∠-110.4146°
	M_{vv}	0.9835∠108.8405°	1.0013∠19.503°	0.976∠0.6473°
$TCR2$	M_{hh}	1.0∠0.0°	1.0∠0.0°	1.0∠0.0°
	M_{hv}	0.0078∠-115.9966°	0.0075∠80.827°	0.0161∠94.6297°
	M_{vh}	0.007∠-36.642°	0.0066∠60.049°	0.0091∠51.6909°
	M_{vv}	1.0314∠109.2796°	0.9995∠18.033°	0.9735∠-0.8264°
$TCR3$	M_{hh}	1.0∠0.0°	1.0∠0.0°	1.0∠0.0°
	M_{hv}	0.0141∠-56.7423°	0.014∠128.2324°	0.0255∠113.1313°
	M_{vh}	0.0109∠-8.9582°	0.0127∠82.5752°	0.016∠73.399°
	M_{vv}	0.9799∠108.6503°	0.9899∠19.3167°	0.9639∠0.4479°
$45°DCR1$	M_{hh}	0.1398∠15.3151°	0.1342∠-172.4335°	0.1203∠-148.8865°
	M_{hv}	1.0∠0.0°	1.0∠0.0°	1.0∠0.0°
	M_{vh}	0.9203∠86.0564°	0.9391∠-12.0094°	0.9788∠1.8672°
	M_{vv}	0.0772∠-91.5725°	0.0633∠-11.4249°	0.0459∠7.1077°
$45°DCR2$	M_{hh}	0.06∠12.8468°	0.0581∠-176.8606°	0.0507∠-147.8115°
	M_{hv}	1.0∠0.0°	1.0∠0.0°	1.0∠0.0°
	M_{vh}	0.9365∠87.6587°	0.9306∠-12.0286°	0.9707∠1.8069°
	M_{vv}	0.0406∠-100.6861°	0.0425∠-22.6459°	0.0255∠4.8021°
$45°DCR3$	M_{hh}	0.0605∠12.5702°	0.0694∠-168.9972°	0.0621∠-141.559°
	M_{hv}	1.0∠0.0°	1.0∠0.0°	1.0∠0.0°
	M_{vh}	0.9679∠88.873°	0.9346∠-11.8745°	0.9745∠1.9538°
	M_{vv}	0.0065∠-145.3458°	0.0164∠-72.4748°	0.007∠151.8828°

at position 11 of the corresponding matrix). Therefore, the relative amplitude and phase characteristics of the VV channel (element at position 22 of the corresponding matrix) of the TCR equipment at different positions represent the range-dependence of the polarization characteristics. The positional distribution of the three TCR image points is shown in Figure 7, in which the abscissa is the range direction and their abscissas are 185, 137, and 53, respectively. Figure 2 shows the amplitude variation of three TCR scattering matrices. Figure 3 shows the corresponding phase variation. Since the ideal polarization scattering matrix of the 45° DCR is $\begin{pmatrix} 0 & 1 \\ 1 & 0 \end{pmatrix}$ [48], we normalize the measured scattering matrix by using the HV channel (element at position 12 of the corresponding matrix). Therefore, the relative amplitude and phase characteristics of the VH channel (element at position 21 of the corresponding matrix) of 45° DCR equipment at different positions represent the range-dependence of the polarization characteristics. The positional distribution of the three 45° DCR image points are shown in Figure 7, in which the abscissa is the range direction and their abscissas are 227, 25, and 101, respectively. Figure 4 shows the amplitude variation of three 45° DCRs

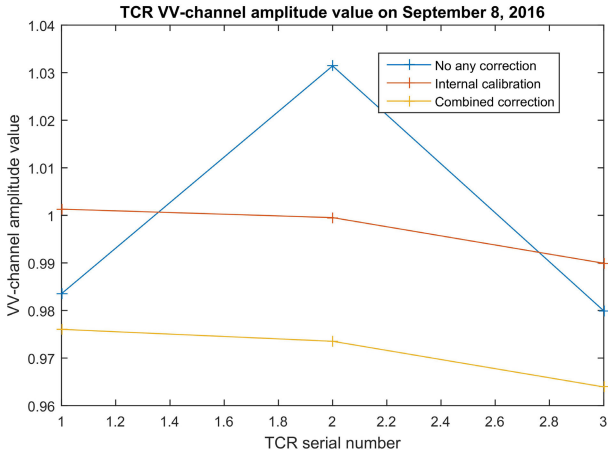

FIGURE 2. TCR VV-channel amplitude value on September 8, 2016.

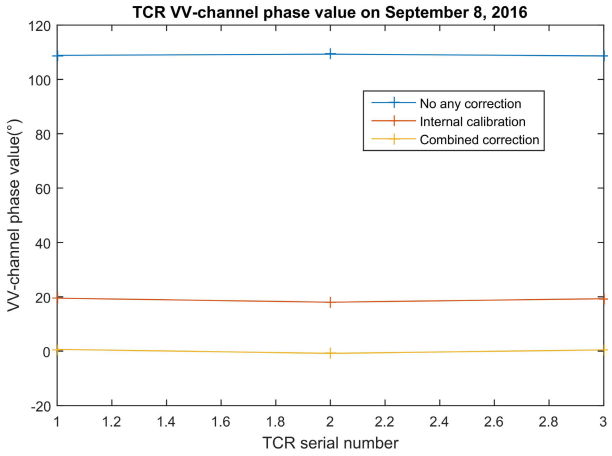

FIGURE 3. TCR VV-channel phase value on September 8, 2016.

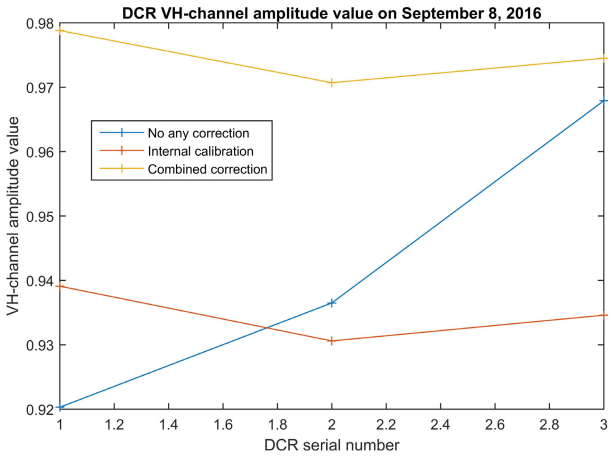

FIGURE 4. 45° DCR VH-channel amplitude value on September 8, 2016.

scattering matrices. Figure 5 shows the corresponding phase variation.

Figure 2 illustrates that the maximum amplitude deviation of the VV channel of the three TCR scattering matrices

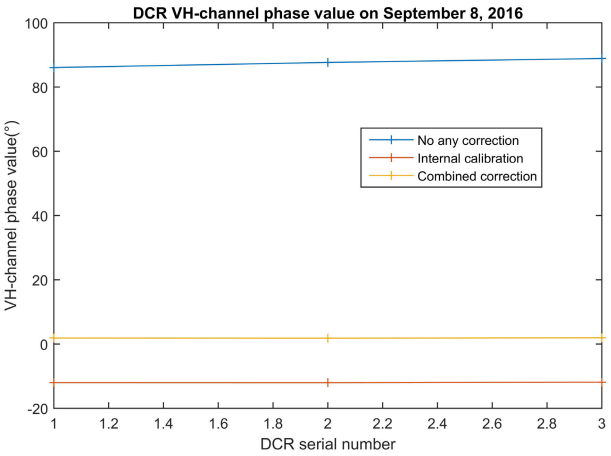

FIGURE 5. 45° DCR VH-channel phase value on September 8, 2016.

improved from 0.44 dB to 0.10 dB after internal calibration correction, and the improvement is over 0.34 dB. From Figure 2 we see intuitively that after calibration of the internal calibration data, the fluctuations of amplitude are greatly eliminated; that is, the internal calibration correction eliminates the range-dependence of VV channel polarization distortion. Figure 4 illustrates that the maximum amplitude deviation of the VH channel of three 45° DCR scattering matrices improved from 0.44 dB to 0.08 dB after internal calibration correction, and the improvement is over 0.36 dB. From Figure 4 we can see intuitively that after calibration of the internal calibration data, the fluctuations of amplitude are greatly eliminated; that is, the internal calibration correction eliminates the range-dependence of VH channel polarization distortion. As can be seen in Figures 3 and 5, the internal calibration process largely corrects the phase error of the channel. Since the overall improvement in phase deviation is around 100°, the improvement of the range-dependence of phase distortion is analyzed from the specific values in Table 1. In particular it can be seen from the phase changes of the VH channels of the three DCRs that the phase inconsistency is improved from 2.8° to 0.15° after the internal calibration process; that is, the internal calibration correction eliminates the range-dependence of VH channel polarization distortion. The phase fluctuations of the VV channel of the three TCRs are already very small, so the effect of the internal calibration process on the phase fluctuations is not apparent. In addition it can be seen in Figures 3 and 5 that, although the internal calibration process greatly improves the phase deviation, there is still a large overall residual phase error. According to previous theory, internal calibration primarily eliminates amplitude and phase errors in a single channel that varies with look-angle. The amplitude and phase errors associated with the polarization characteristics between the channels still require external calibration to be completely eliminated.

In addition it can also be seen that the amplitude and phase of the VV channel of the TCR equipment have moved as a

whole after correcting the obtained parameters for polarimetric distortion in Figure 2 and 3. And it can also be seen that the amplitude and phase of the VH channel of 45° DCR equipment have moved as a whole after correcting the obtained parameters for polarimetric distortion in Figure 4 and 5. In Figures 2, 3, 4, and 5, the resulting curves of the second polarimetric calibration scheme and the third polarimetric calibration scheme are parallel. These intuitively show that the parameters for polarization distortion obtained by external calibration are used to eliminate the polarization distortion of the entire image as a whole; i.e., to eliminate constant polarization distortion or a second type of polarization distortion. In the test on September 8, 2016 the external calibration correction significantly improved the phase imbalance between the HH and VV channels of the TCR equipment and the phase imbalance between the HV and VH channels of 45° DCR equipment. Since the internal calibration accomplished a good correction of the amplitude imbalance, the improvement of the amplitude imbalance by the external calibration is not obvious. In the other three experiments, similarly, the correction of the internal calibration based on the correction of the antenna pattern improves the fluctuation of channel amplitude and phase at different ranges, and the calibration is different at different locations, while the external calibration is a holistic movement of the amplitude and phase characteristics at all locations. And these two kinds of corrections resolve the variable polarization distortion and the constant polarization distortion.

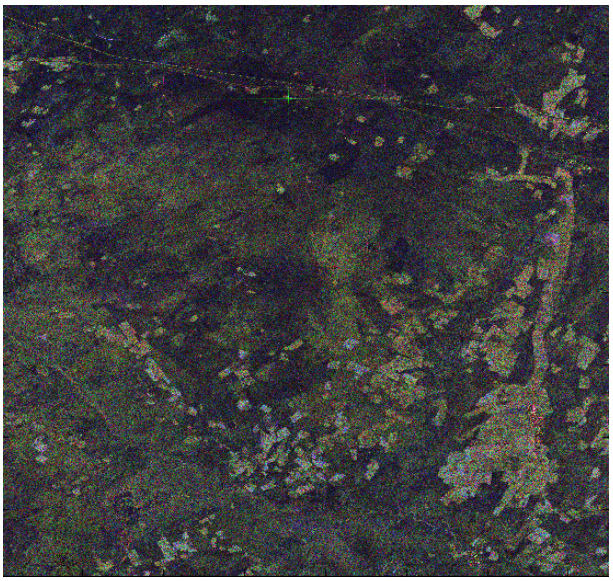

FIGURE 6. Polarized synthesized pseudo color image of the experimental data on September 8, 2016 after two kinds of correction.

In order to intuitively express the correction effect on the polarization, a pseudo-color map synthesis based on Pauli-based object decomposition is performed on the polarization SAR data, and four gray scale images are combined into one color image. Blue is the sum of the co-polarized channels; i.e., $M_{hh} + M_{vv}$; red is the subtraction of the co-polarized channels; i.e., $M_{hh} - M_{vv}$; green is the sum of the cross-polarized channels; i.e., $M_{hv} + M_{vh}$. Figure 6 shows the polarized synthesized pseudo color image of the experimental data on September 8, 2016 after two kinds of correction, and Figure 7 is an enlarged view of the location of the calibration equipment. For comparison Figure 8 shows an enlarged view of the area of the experimental equipment that has been corrected only by internal calibration, and Figure 9 shows the data without any correction. Compare the image points of the three TCRs and three 45° DCRs in Figures 7, 8, and 9. We can intuitively see that after correcting for the internal calibration, the target quality improves, and after the combinatorial correction, the target quality significantly improves. The image points of TCRs become pure blue, which is the color that the TCR should have in the

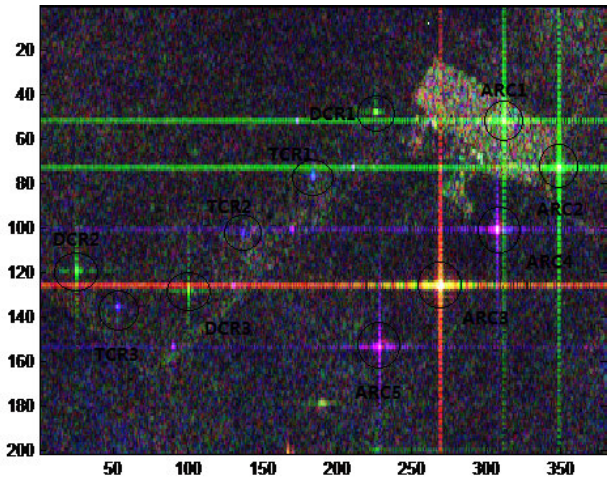

FIGURE 7. The enlarged view of the placement area of the calibration equipment on September 8, 2016 after two kinds of correction. The coordinates of TCR1 are (185, 76), the TCR2 is (137, 103), the TCR3 is (53, 135), the DCR1 is (227, 47), the DCR2 (25, 119), and the DCR3 is (101,128).

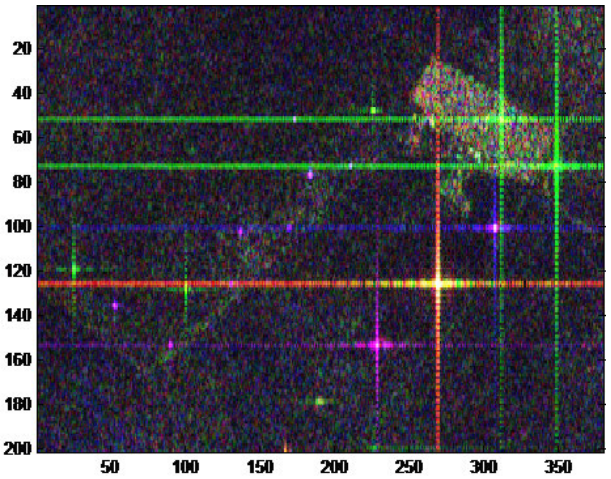

FIGURE 8. The enlarged view of the placement area of the calibration equipment on September 8, 2016 after correction only by internal calibration.

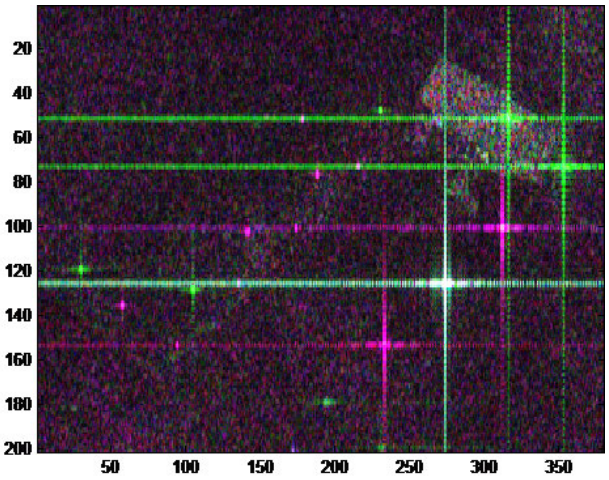

FIGURE 9. The enlarged view of the placement area of the calibration equipment on September 8, 2016 without any correction.

polarized synthesized pseudo color image; and the image points of DCRs become pure green, which is the color that the DCR should have in the polarized synthesized pseudo color image.

V. CONCLUSION

The satellite internal calibration system needs to be sufficiently robust in order to obtain high-precision spaceborne polarimetric SAR data. It is necessary to comprehensively measure the antenna system before launch and to establish the accurate models for the antenna pattern. After the satellite is in orbit the in-orbit antenna pattern data can be obtained based on the internal calibration monitoring data and the previously established model, so that the correction of the variable polarization distortion can be performed. This can greatly reduce the workload of the polarimetric calibration test in the field, reduce the number required for calibration equipment, and improve the accuracy of the polarimetric data product.

However, the antenna pattern correction based on the internal calibration data inversion does not completely eliminate the polarization distortion. It is also necessary to extract the remaining polarization distortion parameters based on the external calibration test of the calibration equipment.

In this paper the strategy for the polarization calibration, based on the combination of internal calibration and external calibration, is used to solve the problem of SAR polarization distortion with the phased array antennas. The strategy does not depend on the distributed target of the previous spaceborne polarization SAR calibration, and only uses a small amount of polarization calibration equipment, which greatly reduces the cost of developing the calibration equipment and the workload of the field test. The strategy for combinatorial polarimetric calibration makes full use of the advantages of the internal and external calibration of the spaceborne polarization SAR with the phased array antenna, and reduces the field workload of the external calibration, and is a very suitable solution for spaceborne SAR polarimetric calibration.

ACKNOWLEDGMENT

The authors would like to thank the GF-3 SAR Satellite Group for the satellite and ground system development work, the staff of the China Center for Resources Satellite Data and Application for their help, and the members of the calibration team for their efforts in deploying equipment at the Erdos calibration site in Inner Mongolia, China.

REFERENCES

[1] A. Freeman, Y. Shen, and C. Werner, "Polarimetric SAR calibration experiment using active radar calibrators," *IEEE Trans. Geosci. Remote Sens.*, vol. 28, no. 2, pp. 224–240, Mar. 1990.

[2] A. Freeman, "A new system model for radar polarimeters," *IEEE Trans. Geosci. Remote Sens.*, vol. 29, no. 5, pp. 761–767, Sep. 1991.

[3] D. Sheen, A. Freeman, and E. Kasischke, "Phase calibration of polarimetric radar images," *IEEE Trans. Geosci. Remote Sens.*, vol. 27, no. 6, pp. 719–731, Nov. 1989.

[4] S. Quegan, "A unified algorithm for phase and cross-talk calibration of polarimetric data-theory and observations," *IEEE Trans. Geosci. Remote Sens.*, vol. 32, no. 1, pp. 89–99, Jan. 1994.

[5] H. Zebker, J. Van Zyl, S. Durden, and L. Norikane, "Calibrated imaging radar polarimetry: Technique, examples, and applications," *IEEE Trans. Geosci. Remote Sens.*, vol. 29, no. 6, pp. 942–961, Nov. 1991.

[6] H. Zebker and J. Van Zyl, "Imaging radar polarimetry: A review," *Proc. IEEE*, vol. 79, no. 11, pp. 1583–1606, Nov. 1991.

[7] M. Satake, T. Kobayshi, T. Manabe, and H. Masuko, "Polarimetric calibration of X-band airborne synthetic aperture radar using corner reflectors and an active radar calibrator," in *Proc. IEEE Int. Geosci. Remote Sens. Symp.*, Seattle, WA, USA, Jul. 1998, pp. 660–662.

[8] E. L. Christensen, N. Skou, J. Dall, K. W. Woelders, J. H. Jorgensen, J. Granholm, S. N. Madsen, "EMISAR: An absolutely calibrated polarimetric L- and C-band SAR," *IEEE Trans. Geosci. Remote Sens.*, vol. 36, no. 6, pp. 1852–1865, Nov. 1998.

[9] T. Ainsworth, L. Ferro-Famil, and J.-S. Lee, "Orientation angle preserving a posteriori polarimetric SAR calibration," *IEEE Trans. Geosci. Remote Sens.*, vol. 44, no. 4, pp. 994–1003, Apr. 2006.

[10] M. Shimada, N. Kawano, M. Watanabe, T. Motooka, and M. Ohki, "Calibration and validation of the Pi-SAR-L2," in *Proc. Conf. Asia–Pacific Conf. Synth. Aperture Radar (APSAR)*, Tsukuba, Japan, Sep. 2013, pp. 194–197.

[11] M. Satake, T. Kobayashi, J. Uemoto, T. Umehara, S. Kojima, T. Matsuoka, A. Nadai, and S. Uratsuka, "Polarimetric calibration of Pi-SAR2," in *Proc. Conf. Asia–Pacific Conf. Synth. Aperture Radar (APSAR)*, Tsukuba, Japan, Sep. 2012, pp. 79–80.

[12] F. Ming, J. Hong, and L. Zhang, "Improved calibration method of the airborne polarimetric SAR," in *Proc. 3rd Int. Asia–Pacific Conf. Synth. Aperture Radar (APSAR)*, Seoul, South Korea, Sep. 2011, pp. 1–3.

[13] M. L. Williams, N. Stacy, D. Badger, M. Preiss, and A. Preiss, "Calibration and performance validation of the ingara, high resolution, fully polarimetric, X-band SAR," in *Proc. CEOS Workshop Polarimetric SAR*, Ulm, Germany, 2004, pp. 27–28.

[14] A. Freeman, "SIR-C calibration results," *Math. Comput. Model.*, vol. 33, nos. 6–7, pp. 695–706, 2001.

[15] H. Kimura, "Calibration of polarimetric PALSAR imagery affected by faraday rotation using polarization orientation," *IEEE Trans. Geosci. Remote Sens.*, vol. 47, no. 12, pp. 3943–3950, Dec. 2009.

[16] G. Sandberg, L. E. B. Eriksson, and L. M. H. Ulander, "Measurements of faraday rotation using polarimetric PALSAR images," *IEEE Geosci. Remote Sens. Lett.*, vol. 6, no. 1, pp. 142–146, Jan. 2009.

[17] R. Touzi and M. Shimada, "Polarimetric PALSAR calibration," *IEEE Trans. Geosci. Remote Sens.*, vol. 47, no. 12, pp. 3951–3959, Dec. 2009.

[18] M. Shimada, "Model–based polarimetric SAR calibration method using forest and surface–scattering targets," *IEEE Trans. Geosci. Remote Sens.*, vol. 49, no. 5, pp. 1712–1733, May 2011.

[19] F. J. Meyer and J. B. Nicoll, "Prediction, detection, and correction of faraday rotation in full–polarimetric L–band SAR data," *IEEE Trans. Geosci. Remote Sens.*, vol. 46, no. 10, pp. 3076–3086, Oct. 2008.

[20] T. Moriyama, "Polarimetric calibration of PALSAR2," in *Proc. IEEE Int. Geosci. Remote Sens. Symp. (IGARSS)*, Milan, Italy, Jul. 2015, pp. 1284–1287.

[21] R. Touzi and M. Shimada, "Calibration and validation of polarimetric ALOS2," in *Proc. IEEE Int. Geosci. Remote Sens. Symp. (IGARSS)*, Milan, Italy, Jul. 2015, pp. 4113–4116.
[22] R. Touzi, R. K. Hawkins, and S. Cote, "High–precision assessment and calibration of polarimetric RADARSAT–2 SAR using transponder measurements," *IEEE Trans. Geosci. Remote Sens.*, vol. 51, no. 1, pp. 487–503, Jan. 2013.
[23] G. L. Iannini and S. Tebaldini, "Long term relative polarimetric calibration by natural targets," in *Proc. IEEE Int. Geosci. Remote Sens. Symp. (IGARSS)*, Melbourne, VIC, Australia, Jul. 2013, pp. 2357–2360.
[24] G. L. Iannini and S. Tebaldini, "Radarsat-2 polarimetric calibration performance over five years of operation," in *Proc. 10th Eur.Conf. Synth. Aperture Radar*, Berlin, Germany, Jun. 2014, pp. 1–4.
[25] K. Sarabandi, L. Pierce, and F. Ulaby, "Calibration of a polarimetric imaging SAR," *IEEE Trans. Geosci. Remote Sens.*, vol. 30, no. 3, pp. 540–549, May 1992.
[26] K. Sarabandi,"Calibration of a polarimetric synthetic aperture radar using a known distributed target," *IEEE Trans. Geosci. Remote Sens.*, vol. 32, no. 3, pp. 575–582, May 1994.
[27] K. Sarabandi, L. Pierce, Y. Oh, M. Dobson, F. Ulaby, A. Freeman, and P. Dubois, "Cross-calibration experiment of JPL AIRSAR and truck-mounted polarimetric scatterometer," *IEEE Trans. Geosci. Remote Sens.*, vol. 32, no. 5, pp. 975–985, Sep. 1994.
[28] J. Van Zyl, "Calibration of polarimetric radar images using only image parameters and trihedral corner reflector responses," *IEEE Trans. Geosci. Remote Sens.*, vol. 28, no. 3, pp. 337–348, May 1990.
[29] A. Freeman, J. Van Zyl, J. Klein, H. Zebker, and Y. Shen, "Calibration of Stokes and scattering matrix format polarimetric SAR data," *IEEE Trans. Geosci. Remote Sens.*, vol. 30, no. 3, pp. 531–539, May 1992.
[30] A. Freeman, M. Alves, B. Chapman, J. Cruz, Y. Kim, S. Shaffer, J. Sun, E. Turner, and K. Sarabandi, "SIR–C data quality and calibration results," *IEEE Trans. Geosci. Remote Sens.*, vol. 33, no. 4, pp. 848–857, Jul. 1995.
[31] K. Sarabandi, L. Pierce, M. Dobson, F. Ulaby, J. Stiles, T. Chiu, R. De Roo, R. Hartikka, A. Zambetti, and A. Freeman, "Polarimetric calibration of SIR–C using point and distributed targets," *IEEE Trans. Geosci. Remote Sens.*, vol. 33, no. 4, pp. 858–866, Jul. 1995.
[32] M. Fujita, T. Masuda, Y. Fujino, and M. Satake, "SIR-C polarimetric calibration by using polarization selective dihedrals and a polarimetric active radar calibrator," in *Proc. 10th Eur. Conf. Synth. Aperture Radar*, Singapore, Aug. 1997, pp. 1941–1943.
[33] T. Moriyama, M. Shimada, and M. Watanabe, "The application of polarimetric calibration using polarimetric scattering characteristics of urban areas to ALOS PALSAR," in *Proc. IEEE Int. Symp. Geosci. Remote Sens.*, Denver, CO, USA, Aug. 2006, pp. 348–351.
[34] T. Moriyama, M. Shimada, and M. Watanabe, "Polarimetric calibration for RADARSAT-2," in *Proc. IEEE Int. Geosci. Remote Sens. Symp. (IGRASS)*, Honolulu, HI, USA, Jul. 2000, pp. 2197–2199.
[35] A. Luscombe, "Plans for radiometric and polarimetric calibration of RADARSAT-2 beams," in *Proc. SAR Workshop: CEOS Committee Earth Observ. Satell.*, vol. 450, 2000, p. 89.
[36] A. Luscombe, "Radarsat-2 calibration: Proposed targets and techniques," in *Proc. IEEE Int. Geosci. Remote Sens. Symp. (IGRASS)*, Sydney, NSW, Australia, Jul. 2001, pp. 496–498.
[37] W. Liang, Z. Jia, X. Qiu, J. Hong, Q. Zhang, B. Lei, F. Zhang, Z. Deng, and A. Wang, "Polarimetric calibration of the GaoFen–3 mission using active radar calibrators and the applicable conditions of system model for radar polarimeters," *Remote Sens.*, vol. 11, no. 2, p. 176, Jan. 2019.
[38] H. A. Zebker, J. J. van Zyl, and D. N. Held, "Imaging radar polarimetry from wave synthesis," *J. Geophys. Res., Solid Earth*, vol. 92, no. B1, pp. 683–701, 1987.
[39] A. Freeman, "SAR calibration: An overview," *IEEE Trans. Geosci. Remote Sens.*, vol. 30, no. 6, pp. 1107–1121, Nov. 1992.
[40] D. Hounam, M. Schwerdt, and M. Zink, "Active antenna module characterisation by pseudo-noise gating," in *Proc. 25th ESA Antenna Workshop Satell. Antenna Technol.*, Noordwijk, The Netherlands, Oct. 2002.
[41] B. Grafmuller, A. Herschlein, and C. Fischer, "The TerraSAR-X antenna system," in *Proc. IEEE Int. Radar Conf.*, Arlington, VA, USA, May 2005, pp. 222–225.
[42] M. Bachmann, M. Schwerdt, B. Brautigam, B. Grafmuller, A. Herschlein, and J. L. Alvarez-Perez, "The TerraSAR-X antenna model approach," in *Proc. 2nd Int. ITG Conf. Antennas*, Munich, Germany, Mar. 2002, pp. 13–142.
[43] Q. Zhang, "System design and key technologies of the GF-3 satellite," *Acta Geod. Cartogr. Sin*, vol. 46, no. 9, pp. 269–277, 2017.
[44] Z. Qingjun and L. Yadong, "Overview of Chinese first C band multi-polarization SAR satellite GF-3," *Aerosp. China*, vol. 18, no. 3, pp. 22–31, 2019.
[45] J. Sun, W. Yu, and Y. Deng, "The SAR payload design and performance for the GF–3 mission," *Sensors*, vol. 17, no. 10, p. 2419, Oct. 2017.
[46] S. Jiang, X. Qiu, B. Han, and W. Hu, "A quality assessment method based on common distributed targets for GF–3 polarimetric SAR data," *Sensors*, vol. 18, no. 3, p. 807, Mar. 2018.
[47] S. Jiang, X. Qiu, B. Han, J. Sun, and C. Ding, "Error source analysis and correction of GF–3 polarimetric data," *Remote Sens.*, vol. 10, no. 11, p. 1685, Oct. 2018.
[48] G. T. Ruck, D. E. Barrick, W. D. Stuart, and C. K. Krichbaum, *Radar Cross Section Handbook*, vol. 1. New York, NY, USA: Plenum Press, 1970.

WEIBIN LIANG was born in Shanxi, China, in 1976. He received the degree from the School of Electronics and Information Engineering, Beijing University of Aeronautics and Astronautics, in April 2004, and the Ph.D. degree from the University of Chinese Academy of Sciences, in June 2019. He joined the Institute of Electronics, Chinese Academy of Sciences, in 2004. He is mainly involved in spaceborne SAR signal processing, system calibration, quality assessment and other research work, the development of spaceborne SAR calibration and quality assessment systems, and the development of calibration equipment.

ZENGZENG JIA was born in Shandong, China, in 1990. He received the degree from the School of Information and Electronics, Beijing Institute of Technology, in June 2016. He joined the Institute of Electronics, Chinese Academy of Sciences, in 2016. He is mainly involved in spaceborne SAR signal and other research work, the development of spaceborne SAR calibration and quality assessment systems, and the development of calibration equipment.

JUN HONG was born in 1960. He received the bachelor's degree from the University of Science and Technology of China. He came to work with the Institute of Electronics, the Chinese Academy of Sciences, in 1983. He is currently a Researcher and a Ph.D. Supervisor. He is mainly engaged in research on the novel SAR system and calibration technology, microwave quantitative remote sensing data application and other aspects.

QINGJUN ZHANG was born in Jiangsu, China, in 1969. He received the Ph.D. degree from the Huazhong University of Science and Technology. He joined the Overall Design Department, China Academic of Space Technology (CAST). He is mainly involved in space satellite remote sensing program, and had token part in several optical microwave and SAR satellite remote sensing system, and including CBERS HY-2 and GF-3.

AICHUN WANG received the B.S. degree in automation from the China University of Geosciences, Wu Han, in 2005, the M.Sc. degree in flight vehicle design from the China Academy of Space Technology, in 2009, and the Ph.D. degree in signal and information processing from The University of Chinese Academy of Sciences, in 2017. He joined the China Centre for Resources Satellite Data and Application, in 2009. His current research interest is multibaseline InSAR data processing, calibration and its applications.

ZHAOGUO DENG was born in 1994. He received the bachelor's degree from the Beijing Institute of Technology (BIT), in 2016, and the master's degree from the Information College of BIT, in 2018. He joined with the Institute of Electronics of the Chinese Academy of Sciences, in 2019. He is mainly involved in the research of SAR calibration and assessment.